한국환경과학회지 제16권(제5호), 541~548, 2007
*Journal of the Environmental Sciences*

# A Simple Simulation of Parabola-Shaped Clouds in the Lee of a Low Bell-Shaped Mountain Using the ARPS

**Seung-Jae Lee, Hwa-Woon Lee* and Sung-Dae Kang****
*Numerical Weather Prediction Division, Korea Meteorological Administration, Seoul 156-720, Korea*
**Department of Atmospheric Sciences, Pusan National University, Busan 609-735, Korea*
***System Division, APEC Climate Center, Busan 611-705, Korea*
*(Manuscript received 28 September, 2006; accepted 3 February, 2007)*

A three-dimensional linear model and the Advanced Regional Prediction System (ARPS) were used to simulate parabola-shaped disturbances and clouds in the lee of a bell-shaped mountain. The ARPS model was compared in the x-y plane against the linear model's analytic solution. Under similar conditions with the linear theory, the ARPS produced well-developed parabola-shaped mountain disturbances and confirmed the features are accounted for in the linear regime. A parabola-shaped cloud in the lee of an isolated bell-shaped mountain was successfully simulated in the ARPS after 6 hours of integration time with the prescribed initial and boundary conditions, as well as a microphysical scheme.

Key Words : Mountain wave, Linear model, Fast Fourier Transform, ARPS, Lee clouds, Froude number

## 1. Introduction

Mountain internal gravity wave (IGW) is generated when a stably-stratified fluid passes over a mountainous terrain. This phenomenon is one of the meso-β scale atmospheric events[1]. This is a density-stratified flow past mountains and can be accounted for by non-dimensional mountain half-width $\hat{a}=Na/U$ or mountain height $\hat{h}=NH/U$ ($N$: Brunt- Väisäla frequency; $a$: mountain half-width; $H$: maximum height of topography; $U$: inflow velocity). $\hat{h}$ is the same as the inverse of Froude number defined by $Fr=U/NH$. Previous researches show that this flow is linear when the $\hat{h}\ll 1$ ($Fr\gg 1$), otherwise it is non-linear when the $\hat{h}\gg 1$ ($Fr\ll 1$). The flow is hydrostatic(nonhydrostatic) if $\hat{a}\gg 1(\hat{a}\ll 1)$. Kármán vortices and cloud streets are typical phenomena generated by non-linear disturbances in the lee of obstacles[7,8] while parabola-shaped disturbances are the results of linear wave disturbances[23]. All waves including mountain waves are oftentimes invisible but can be visualized sometimes in the form of clouds[3,16]. Figure 1 shows the image of parabola-shaped cloud created in the lee of an isolated mountain.

Analytical theories explaining mountain waves include linear, finite amplitude and hydraulic theories. The finite amplitude theory is proper for describing high-energy events like large amplitude mountain waves and downslope windstorms[12,13,18]. On the other hand, the hydraulic theory is commonly used to describe shallow water waves using shallow water equations. Hydraulic theory was first used by Long[14] to represent downslope winds. The linear theory is appropriate in showing the basic gravity wave responses to steady flow passing over a small obstacle in a continuously stratified fluid. Studies of mountain waves as a three dimensional phenomenon are relatively rare in the literature[20,24,25]. Wurtele[26], for the first time, computed vertical velocities in three dimensions for the lee of an isolated mountain.

For mathematical simplicity, linear theory assumes a uniform incoming flow and constant static stability profiles. Authors who have used such conditions include Lyra[15] and Queney[21,22] for two dimensional

Corresponding Author : Seung-Jae Lee, Numerical Weather Prediction Division, Korea Meteorological Administration, Seoul 156-720, Korea
Phone: +82-2-2181-0477
E-mail: email.seungjae.lee@gmail.com

Fig. 1. A parabola-shaped cloud in the lee of an isolated bell-shaped mountain. This is a good evidence of linear mountain wave activities (Fr≫1) in our atmosphere. (Taken from Wurtele[26])

barriers, and Wurtele[26], Crapper[2], Smith[23] and Phillips[17] in the three dimensional case. Phillips[17] did a similar work for an elliptical mountain. Hu et al.[5] evaluated analytic solutions to the nonhydrostatic and hydrostatic forms of Long's model under two types of lower boundary conditions and the same upper boundary condition. He concluded that the significance of the effect of the hydrostatic balance assumption on the solutions of Long's model depends not only on the inclusion of this assumption in the model, but also on the actual vertical boundary conditions used in the solution evaluation.

The purpose of this study is to simulate disturbances induced by mountain wave using an linear model and the ARPS, respectively. The linear mountain-wave solution will be used for the comparison with the ARPS, a complicated non-linear model. Until now, such validation tests used two-dimensional approach in the x-z plane for mountain wave validation experiments[27]. Thus, evaluation of the ARPS results for the simulation of mountain wave disturbance will be presented in the x-z horizontal plane. In Section 2, a three-dimensional linear model is reviewed to understand mountain wave disturbances over an ideal terrain. In Section 3, the ARPS is compared against the linear model solution. The experimental design for a numerical simulation of a parabola-shaped cloud in the lee of an isolated bell-shaped mountain is also described. And finally, Section 4 summarizes this paper.

## 2. Analytical Simulation

### 2.1. Governing equations

For the theoretical description of linear mountain waves, a steady flow of a vertically-unbounded, incompressible and stably-stratified Boussinesq fluid, over small-amplitude topography given by $z=h(x,y)$, is considered. The perturbations to the background wind, pressure and density fields are expressed by the following linearized governing equations:

$$\rho_0 U\frac{\partial u'}{\partial x} = -\frac{\partial p'}{\partial x}, \tag{1}$$

$$\rho_0 U\frac{\partial v'}{\partial x} = -\frac{\partial p'}{\partial y}, \tag{2}$$

$$\rho_0 U\frac{\partial w'}{\partial x} = -\frac{\partial p'}{\partial z} - \rho' g, \tag{3}$$

$$\frac{\partial u'}{\partial x}+\frac{\partial v'}{\partial y}+\frac{\partial w'}{\partial z} = 0, \tag{4}$$

$$\rho' = -\frac{d\bar{\rho}}{dz}\eta, \tag{5}$$

where $x$, $y$ and $z$ are the downstream, cross stream and vertical coordinates; $u'$, $v'$, $w'$, $\rho'$, $p'$, and $\eta$ are the corresponding perturbation velocity components and the perturbation density, pressure and vertical displacement; and $\rho_0$, $U$, and $d\bar{\rho}/dz$ are the background mean density, wind speed, and vertical density gradient, respectively.

Using the kinematic condition for steady flow

$$w' = \frac{d\eta}{dt} \approx U\frac{\partial \eta}{\partial x}, \tag{6}$$

and with $U$ taken as a constant, the system of governing eqs. (1) to (5) can be reduced to a single equation for $\eta(x,y,z)$ the vertical displacement of fluid parcel, or a density surface, above its undisturbed level

$$\frac{\partial^2}{\partial x^2}(\nabla^2\eta) + S^2\nabla^2_{\eta=0H} \tag{7}$$

where

$$S^2\equiv\frac{N^2}{U^2},\ N^2\equiv-\frac{g}{\rho_0}\frac{d\bar{\rho}}{dz},\ \text{and}$$

$$\nabla^2=\frac{\partial^2}{\partial x^2}+\frac{\partial^2}{\partial y^2}+\frac{\partial^2}{\partial z^2}=\nabla^2+\frac{\partial^2}{\partial z^2}H.$$

$S^2$ and $N^2$ are the Scorer parameter describing the vertical structure of the disturbance and the square of the Brunt-Väisälä frequency, respectively. In this paper, $S$ is constant for all cases because the basic wind is uniform. $N$ is likewise set constant in the horizontal and vertical.

Now, the general solution of eq. (7) can be expressed as a double Fourier integral

$$\eta(x,y,z)=\int\int_{-\infty}^{\infty}\hat{h}(k,l)e^{im(k,l)z}e^{i(kx+ly)}dkdl \qquad (8)$$

where

$$\hat{h}(k,l)=\frac{1}{4\pi^2}\int\int_{-\infty}^{\infty}h(x,y)e^{-i(kx+ly)}dxdy, \qquad (9)$$

$$m^2=\frac{(k^2+l^2)}{k^2}(S^2-k^2) \text{ for nonhydrostatic case, and} \qquad (10)$$

$$m=\frac{N}{U}\frac{(k^2+l^2)^{1/2}}{k} \text{ for hydrostatic case.} \qquad (11)$$

For $S^2<k^2$ the positive imaginary root of eq. (10) must be chosen to reflect exponential decay of the disturbance amplitude with height, and for $S^2>k^2$ the sign of $m$ must be chosen to be the same as the sign of $k$ in order to satisfy the radiation condition aloft. To evaluate eq. (8), a two-dimensional finite FFT algorithm is used[23]. Once the vertical displacement $\eta$ is determined with the help of this technique, the other dependent variables can be calculated simultaneously from the basic equations (6), (3), (1) and (2).

2.2. Test results

Fig. 2 shows examples of the three-dimensional (3D) vertical displacements of stably-stratified flows at two levels (1 km and 3 km) over an isolated bell-shaped mountain given by

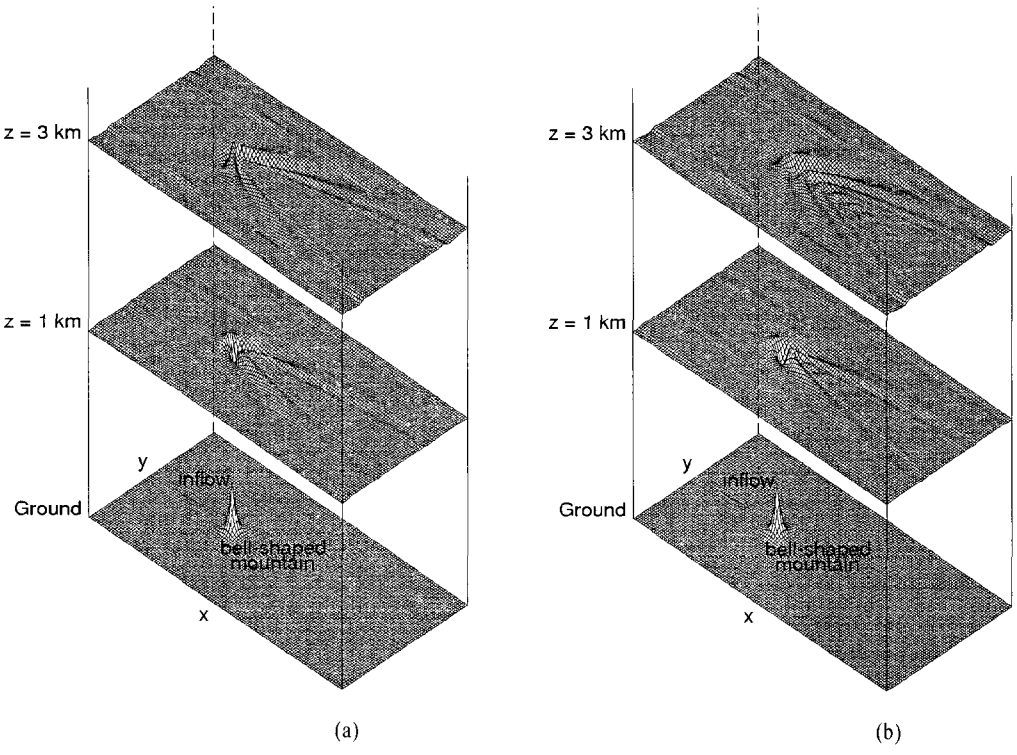


Fig. 2. The vertical displacement $\eta(x,y,z)$ by linear mountain wave disturbances at two levels over (a) large ($a$=5 km) and (b) small ($a$=1 km) bell-shaped mountains. The nonhydrostatic forms of the vertical wave number $m$ is used. The inflow velocity and buoyancy frequency was given $U$=10 m s$^{-1}$ and $N$=0.014 s$^{-1}$, respectively. (Taken from Lee and Lee[11])

$$h(x,y)=\frac{h_m}{(1+r^2/a^2)^n},\ n=1$$

where $r^2=x^2+y^2$, $x$ and $y$ are the distance from the center of the mountain, $a$ is the horizontal mountain scale, and $h_m$ is the mountain height[11]. A sampling interval $dx(=dy)$ is 3 km and the number of grid points is 128 by 64 in the x and y direction. In this case, the patterns of the vertical displacements were computed with the non-hydrostatic form of the vertical wave number $m$, typical atmospheric values of $U$=10 m $s^{-1}$ and $N$=0.014 $s^{-1}$ were chosen.

Figures 2a and b show the patterns of the vertical displacements at the two levels associated with mountain wave disturbances in cases of a large mountain ($a$=5 km) and small one ($a$=1 km), respectively. We can see that at a given height the wave disturbance is in parabola-shaped, and this parabola becomes wider with height. Especially, features of well-developed horse-shoe vortices can be seen at 1 km level. These disturbances are caused by mountain drag associated with the higher pressure on the upwind slopes compared with the downwind as distinguished from the surface friction. In case of a very small hill, there are no wave motions in the horizontal and vertical, and the flow have maximum amplitude just above the mountain top (not shown here).

## 3. Numerical Simulation

### 3.1. The ARPS

The numerical model used is the Advanced Regional Prediction System (ARPS) version 4.3.2b, which was developed at the Center for Analysis and Prediction of Storms (CAPS) at the University of Oklahoma[27]. The ARPS is a non-hydrostatic atmospheric prediction model, which is appropriate for use on scales ranging from a few meters to hundreds of kilometers. It is based on compressible Navier-Stokes equations describing the atmospheric flow, and uses a generalized terrain-following coordinate system. A variety of physical processes are taken into account in the model system. This general purpose and compressible model is designed for storm and other meso-scale atmospheric simulations in real-time prediction on both conventional scalar/vector as well as parallel computers[6]. The dynamics framework consists of prognostic equations for momentum, heat (potential temperature), mass (pressure), water substances, subgrid-scale turbulent kinetic energy (TKE) and the equation of state. All of them are expressed in a fully conservative form in a curvilinear coordinate system which is orthogonal in the horizonal. The continuous equations are solved numerically on an Arakawa C-grid using a split-explicit time integration scheme[10] in a rectangular computational space. Scalars are defined at the center of the grid boxes and the normal velocity components defined on the corresponding box faces.

In the ARPS, wind components and state variables are defined as the sums of base-state variables and deviations from the base state. The base state is assumed to be horizontally homogeneous, time invariant and hydrostatically balanced. For this reason, the base-state mass and wind fields are, in general, not in geostrophic balance, except when the base-state winds are zero. The details of the model can be found in the ARPS User's Guide[27].

### 3.2. Comparison with analytic solution

In this subsection, the ARPS was compared with analytic solutions for model validation. It has been tested using two-dimensional analytic solutions of mountain waves[20,27], but comparison with 3D mountain wave solutions is scarcely conducted up to now. Kang[7] investigated the mechanism of two nonlinear disturbances in the lee of an isolated mountain, Kármán vortex and cloud streets, using a Local Circulation Model and the Regional Atmospheric Modeling System, respectively[9,19]. He checked the accuracy of LCM by comparing the numerical results of low mountain case with linear solution of Smith[23].

To facilitate the comparison of numerical results with analytic solutions, several approximations are made to the original equations used in the ARPS.

- The Boussinesq approximation is imposed by setting the base state density to constant ($\rho_0$) everywhere, except the buoyancy term in the vertical momentum equation. The base state pressure is expressed as a function only of height and is assumed in hydrostatic balance.
- Only the 1st-order terms in the linearized buoyancy terms are used. Incompressibility assumption

is made in the buoyancy term such that the thermal buoyancy $g\theta'/\bar{\theta}$ is identical to $-g\rho'/\rho_0$, as in the linear model of Section 2. Thus, the atmosphere is horizontally and vertically homogeneous.

- The full pressure equation is replaced by the anelastic continuity equation. Because there is no option for hydrostatic or incompressible system in the ARPS, the code of the ARPS was modified to force the incompressibility constraint by removing the pressure advection term. This allows only the partial time derivative with respect to perturbation pressure which is small. Eliminating the pressure advection does not in itself imply incompressibility for time-dependent calculations, but removing the pressure advection does imply incompressibility at steady state. Thus, for steady flow, the approximation leads to model calculations that are strictly incompressible. Though not entirely physical, this approximation is to some extent valid since the largest term in the pressure equation is the divergence term, which is higher by a few orders of magnitude.
- The constant static stability atmosphere with a uniform ambient wind is assumed to represent the simple situation found in the linear theories. The mountain is low (so the wave amplitude is essentially linear) and wide (so that the flow is nearly hydrostatic).

The computational domain is a rectangle, shown in Fig. 3 covering 131 by 67 grid points (128 by 64 for the linear model) in the x and y directions, respectively ($\Delta$x=$\Delta$y=3 km). The model atmosphere is divided into 67 levels with uniform interval of 200 m. Klemp-Lilly-Durran radiation condition is adopted for windward/leeward lateral boundaries, while periodic boundary condition is imposed on the side boundaries in y-direction. The bottom boundary is assumed as a free-slip rigid wall. The top boundary is treated carefully since IGWs propagate upward and reflect in this region. In this section, Orlanski formulation with additional vertical averaging, calculated after Durran and Klemp[4] is employed for the top boundary. This technique is known to improve the results in the tests with linear mountain waves and gravity wave propagation cases[27].

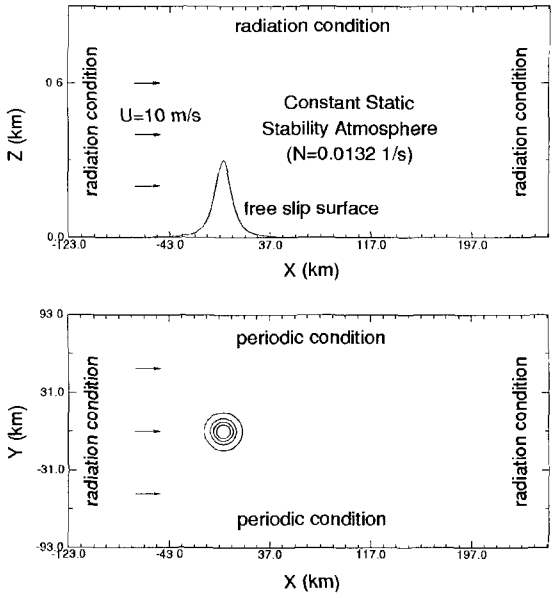


Fig. 3. Boundary and initial conditions used to simulate parabola-shaped disturbances in the lee of a circular mountain using the ARPS. In this case, Fr is 2.525 and the ground potential temperature is 280 K.

Fourth-order (second-order) finite differencing of the advection terms is used in the horizontal (vertical). The Coriolis force and surface drag are neglected since they play insignificant roles on the mechanical motions of mountain wave disturbances. The 1.5 TKE turbulent mixing and isotropic divergence damping are selected for a vertical mixing and acoustic wave divergence damping options, respectively. A sponge layer is constructed using a Rayleigh friction, which has a coefficient prescribed $\nu(z) = (\nu_t/2)[1 - cos\ \pi(z - z_b)/(z_t - z_b)]$ in the sponge layer, where $z_b$ is the height of the bottom of the sponge layer, $z_t$ the height of the top of the domain, and $\nu_t$ the maximum Rayleigh friction coefficient. In this case, the following parameters have been adopted: $z_b$=8 km, $z_t$=12.3 km, $\nu_t$=0.0083 $s^{-1}$. The inverse of $\nu_t$ is 20 times the large time step (6.0 s), as recommended by Xue et al.[27].

In this experiment, the Froude number is 2.525, which satisfies the linear regime. The Klemp-Durran upper boundary condition is exact for the case of linear hydrostatic gravity waves. Thus, if we are trying to match a linear solution in the hydrostatic re-

gime, then we do not need to include a sponge layer. However, in this case, a mountain height 300 m is somewhat large and the Froude number 2.525 is not so big for a linear mountain wave regime. Therefore, we still put a sponge layer above the mountain in this simulation.

Figure 4 shows the comparison of numerical results from the ARPS with analytic solutions from the linear model. Overally, the numerical and analytic solutions agree with each other, and they are consistent. Basically, this indicates the phenomena can be explained in the linear regime using linear theory. Especially, the downward motions match very closely, but the contours of upward motions are somewhat overestimated by the numerical model. The difference between the two models as depicted by the contour shape is due to the hydrostatic assumption and incompressibility constraint in the linear model and the initialization procedure in the ARPS.

Also, nonlinearity (Fr=2.525) is a possible source of the discrepancy between the FFT results and the ARPS calculations. If a mountain height that is small enough to eliminate the nonlinear effects is used, the two models will be more matched.

### 3.3. Parabola-shaped clouds in the lee of an isolated bell-shaped mountain

Simulation of a parabola-shaped cloud observed in the lee of an isolated bell-shaped mountain is carried out. Most parameters are similar with the previous subsection except for equation formulations. The second order terms and total density are used in the linearized buoyancy and pressure gradient force terms, respectively. Original formulation as described in ARPS 4.0 User's Guide for pressure equation is used. The Boussinesq approximation is not adopted in the simulation. Anisotropic divergence damping is selected for acoustic wave divergence damping options. Kessler microphysics parameterization scheme is used for the cloud formation in the model.

The vertical profiles of ground-relative wind, potential temperature and specific humidity are shown in Fig. 5. The basic wind is westerly and its speed increases linearly with height from 2 m $s^{-1}$ at the ground up to $z$=500 m. Above 500 m, there is no

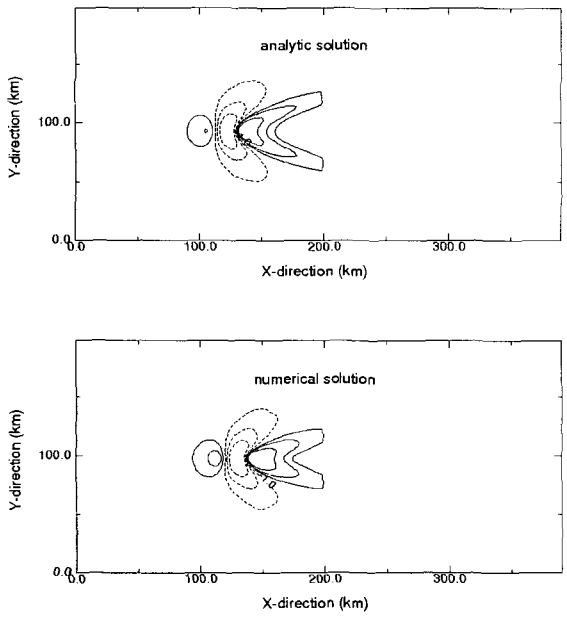


Fig. 4. Horizontal cross sections of the vertical velocity from the ARPS and linear model at $Ul\alpha$=21.6. The vertical velocity is taken at 1.1 km and the contours with the values of -7, -3, -1, +1, +2, +4 cm $s^{-1}$ are plotted. Dashed contours indicate downward motions.

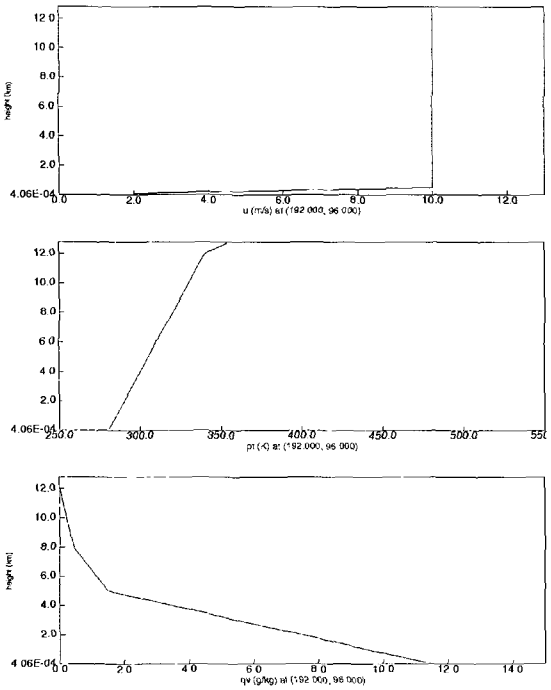


Fig. 5. Wind (m $s^{-1}$), potential temperature (K) and specific humidity (g $kg^{-1}$) profiles used in the numerical simulation of the parabola-shaped clouds in the lee of a circular mountain.

vertical wind shear. Water vapor decreases linearly at the rate of 2 g $kg^{-1}$ $km^{-1}$ from a base value of 11.5 g $kg^{-1}$ up to $z$=5 km, from the level, 0.36 g $kg^{-1}$ up to $z$=8 km approaching to 0 g $kg^{-1}$ at 12 km. Potential temperature increases with height at 10 K $km^{-1}$ from the base state of 280 K up to 12 km, so that strong stability exists, and then 20 K $km^{-1}$ in the stratosphere. These initial conditions are based on Kang and Kimura[8].

Figure 6 shows the evolution of cloud water mixing ratio at the height of 1.1 km at integration time 5.0, 5.5 and 6.0 hours. A parabola-shaped and well-developed cloud in the lee of a circular mountain is successfully simulated after 6 hours. The feature is similar to those commonly observed in the atmosphere. The cloud formed when the model is almost at the steady state condition. The cloud shape is formed as a result of mountain wave activities, which are almost linear disturbances as in the hydrostatic 3D model (see Figs. 1, 2 and 4).

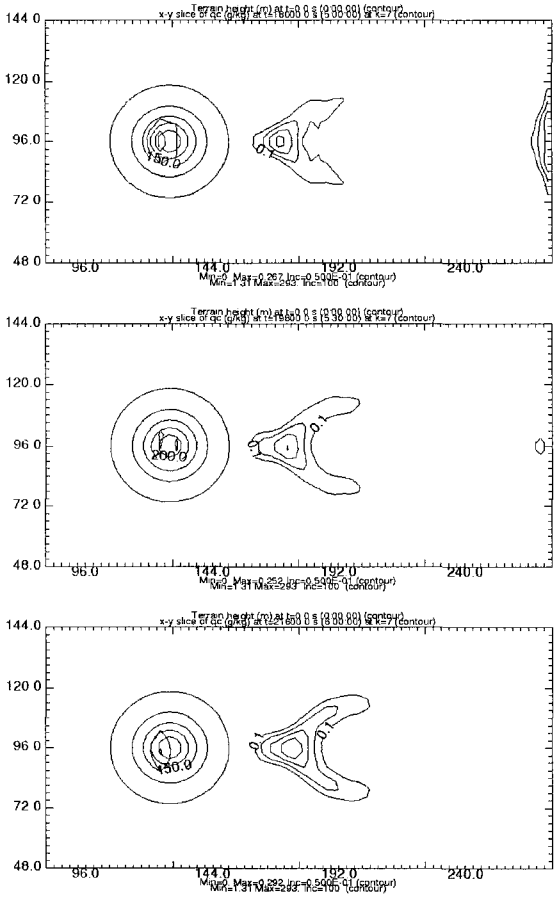


Fig. 6. Horizontal cross sections of cloud water mixing ratio (contours) at 1.1 km at integration time 5.0, 5.5 and 6.0 hours.

## 4. Conclusions

In this study, we intended to simulate a parabola-shaped cloud caused by mountain wave disturbances past a bell-shaped mountain. First, a 3D linear model was used to analytically simulate the airflow over small-amplitude mountains. This linear model treats only the mechanical disturbances without heat source, and the solutions are obtained by using a FFT method. The linear model provided fundamental insight into the underlying dynamics and showed reasonably the occurrence and basic features of the mountain wave disturbance. Because there would be no wave disturbance like Fig. 1 without mountain, the analytical simulation confirmed again that the parabola-shaped cloud can be generated only by mechanical effect of the circular mountain.

Second, the ARPS was adopted for the non-linear numerical simulation of parabola-shaped clouds induced by mountain wave disturbances. For the simulation, the ARPS was simplified and compared against a 3D linear mountain wave solution. Validation tests of the ARPS for *three-dimensional* linear mountain wave disturbance are carried out for the first time. It is shown that the ARPS is able to reproduce the linear results closely when the system of equations is simplified. The well-developed parabola-shaped cloud in the lee of a circular mountain was successfully simulated using the prescribed model initial and boundary conditions after 6 hours. The resulting patterns are similar to those observed in the atmosphere.

## References

1) Atkinson B. W., 1981, Meso-scale Atmosphere. Academic Press, London, 495pp.
2) Crapper G. D., 1959, A three-dimensional solution for waves in the lee of mountains, J. Fluid Mech., 6, 51-76.
3) Doyle J. D., Durran D. R., 2002, The dynamics of mountain-wave-induced rotors, J. Atmos. Sci., 59, 186-201.

4) Durran D. R., Klemp J. B., 1983, A compressible model for the simulation of moist mountain waves, Mon. Wea. Rev., 111, 2341-2361.
5) Hu Q., Reiter E. R., Pielke R. A., 1980, Analytic solutions to Long's model: A comparison of non-hydrostatic and hydrostatic cases, Meteorol. Atmos. Phys., 39, 184-196.
6) Johnson K. W., Bauer J., Riccardi G. A., Droegemeier K. K., Xue M., 1994, Distributed processing of a regional prediction model, Mon. Wea. Rev., 122, 2558-2572.
7) Kang S. D., 1997, A numerical study on the mesoscale disturbance in the lee of an isolated mountain, Ph.D. dissertation, Dept. of Geoscience, University of Tsukuba, 113pp.
8) Kang S. D., and Kimura F., 1997, A numerical study on the mechanism of cloud-street formation in the lee of an isolated mountain near a coast, J. Meteor. Soc. Japan, 75, 955-968.
9) Kikuchi T., Arakawa S., Kimura F., Shirasaki K., Nagano T., 1981, Numerical study on the effects of mountains on the land and sea breeze circulation in the Kanto district, J. Meteor. Soc. Japan, 59, 723-737.
10) Klemp J. B., Wilhelmson R. B., 1978, The simulation of three-dimensional convective storm dynamics, J. Atmos. Sci., 35, 1070-1096.
11) Lee S. J., Lee H. W., 2006, A three-dimensional linear mountain wave model and its application to complex terrain, J. Korean Meteor. Soc., 42, 1-10.
12) Lilly D. K., 1978, A severe downslope windstorm and aircraft turbulence event induced by a mountain wave, J. Atmos. Sci., 35, 59-77.
13) Lilly D. K., Klemp J. B., 1980, Comments on the evolution and stability of finite-amplitude mountain wave. Part II: Surface wave drag and severe downslope windstorms, J. Atmos. Sci., 37, 2119-2121.
14) Long R. R., 1953, Some aspects of the flow of stratified fluids. I. A theoretical investigation, Tellus, 20, 386-390.
15) Lyra G., 1943, Theorie der stationaren leewellen stromung in freier atmosphare, Z. Ang. Math. Mech., 23, 1-28.
16) Neiman P. J., Shaw J. A., 2003, Coronas and iridescence in mountain wave clouds over northeastern Colorado, Bull. Amer. Met. Soc., 84, 1373-1386.
17) Phillips D. S., 1984, Analytical surface pressuer and drag for linear hydrostatic flow over three-dimensional elliptical mountains, J. Atmos. Sci., 41, 1073-1084.
18) Peltier W. R., Clark T. L., 1979, The evolution and stability of finite-amplitude mountain waves. Part II. Surface wave drag and severe downslope windstorms, J. Atmos. Sci., 36, 1498-1529.
19) Pielke R. A., Cotton W. R., Walko R. L., Tremback C. J., Nicholls M. E., Moran M. D., Wesley D. A., Lee T. J., Copeland J. H., 1992, A comprehensive meteorological modeling system-RAMS, Meteor. Atmos. Phys., 49, 69-91.
20) Pinty J., Benoit R., Richard E., Laprise R., 1995, Simple tests of a semi-implicit semi-lagrangian model on 2D mountain wave problems, Mon. Wea. Rev., 123, 3042-3058.
21) Queney P., 1947, Theory of perturbations in stratified currents with application to air flow over mountain barrier, University of Chicago, Department of Meteorology, Miscellaneous Report no. 23.
22) Queney P., 1948, The problem of air flow over mountains: a summary of theoretical studies, Bull. Amer. Met. Soc., 29, 16-26.
23) Smith R. B., 1980, Linear theory of stratified hydrostatic flow past an isolated mountain, Tellus, 32, 348-364.
24) Wang T. A., Lin Y. L., 1999a, Wave ducting in a stratified shear flow over a two-dimensional mountain. Part I: General linear criteria, J. Atmos. Sci., 56, 412-436.
25) Wang T. A., Lin Y. L., 1999b, Wave ducting in a stratified shear flow over a two-dimensional mountain. Part II: Implications for the development of high-drag states for severe downslope windstorms, J. Atmos. Sci., 56, 437-452.
26) Wurtele M., 1957, The three-dimensional lee wave, Beitr. Phys. Frei. Atmos., 29, 242-252.
27) Xue M., Droegemeier K. K., Wong V., Shapiro A., Brewster K., 1995, Advanced Regional Prediction System (ARPS) Version 4.0 Users's Guide, Center for Analysis and Prediction of Storms, 320pp.